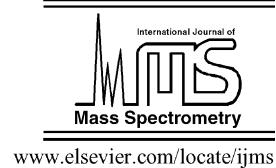




ELSEVIER

International Journal of Mass Spectrometry 223–224 (2003) 805–811



www.elsevier.com/locate/ijms

Subject index Volume 223–224

Accelerator mass spectrometry

Accelerator mass spectrometry of heavy long-lived radionuclides, 713

Acetone

Detection of gaseous oxygenated hydrocarbons in upper tropospheric and lower stratospheric aircraft borne experiments, 733

Acetonitrile cation

Surface collisions of the acetonitrile molecular ion: evidence for isomerization of CD_3CN^+ to the ketenimine cation $\text{CD}_2=\text{C}=\text{ND}^{+*}$, 279

Acetylene

A photoionization mass spectrometric study of acetylene and ethylene in the VUV spectral region, 67

Activation energy

Effect of temperature on dissociative electron attachment to CCl_2F_2 , 217

Aeronomy

UV and low energy electron impact study of electronic state spectroscopy of CF_3I , 647

Alkali ion emitter

Mass spectrometric study of $\text{K}^+ + \text{C}_60$ collisions, 695

Aminophosphonic acids

Gas-phase complexes: noncovalent interactions and stereospecificity, 159

Anion kinetics

A temperature-dependent selected ion flow tube study of anions reacting with SF_5CF_3 , 403

APCI-TOFMS

Evaluation of three gas chromatography and two direct mass spectrometry techniques for aroma analysis of dried red bell peppers, 55

Aroma

Breath-by-breath analysis of banana aroma by proton transfer reaction mass spectrometry, 743

Association

Selected ion flow tube study of NH_4^+ association and of product switching reactions with a series of organic molecules, 459

Atmospheric pressure chemical ionization mass spectrometry (AP-CIMS)

Atmospheric pressure chemical ionization mass spectrometry for the detection of tropospheric trace gases: the influence of clustering on sensitivity and precision, 771

Atmospheric trace gas

Sensitivity and specificity of atmospheric trace gas detection by proton-transfer-reaction mass spectrometry, 365

Attachment

A three-step model applied to free electron attachment to C_60 , Buckminsterfullerene, 447

Banana

Breath-by-breath analysis of banana aroma by proton transfer reaction mass spectrometry, 743

BEB

Calculation of electron impact ionization cross sections of DNA using the Deutsch–Märk and Binary–Encounter–Bethe formalisms, 599

Benzene

The gas-phase chemistry of iron cations coordinated to benzene and the extended aromatic coronene, 411

Breath-by-breath analysis

Breath-by-breath analysis of banana aroma by proton transfer reaction mass spectrometry, 743

Buckminsterfullerene

A three-step model applied to free electron attachment to C_60 , Buckminsterfullerene, 447

CH_4^+

Reactions between CH_4^+ and $\text{C}_2\text{H}_5\text{OH}$, 81

Charge reversal

State selectivity in collisional electron-transfer processes involving the NO molecule, 169

Charge transfer

The charge-excitation exchange process: $\text{He}^+({}^2\text{S}) + \text{Ar}^*({}^3\text{P}) \rightarrow \text{He}^*({}^3,1\text{S}) + \text{Ar}^+({}^2\text{P})$, 327

Charge-excitation exchange

The charge-excitation exchange process: $\text{He}^+({}^2\text{S}) + \text{Ar}^*({}^3\text{P}) \rightarrow \text{He}^*({}^3,1\text{S}) + \text{Ar}^+({}^2\text{P})$, 327

Chemical reaction

Bond-forming reactivity between CF_3^{2+} and H_2/D_2 , 547

Chirality

Gas-phase complexes: noncovalent interactions and stereospecificity, 159

Chlorine

Production of Cl^- via dissociative electron attachment to Cl_2 , 661

Chlorofluorocarbons

Reactions of H_3O^+ with a number of bromine containing fully and partially halogenated hydrocarbons, 627

$\text{C}_2\text{H}_5\text{OH}$

Reactions between CH_4^+ and $\text{C}_2\text{H}_5\text{OH}$, 81

Chromatography

Direct mass spectrometry of complex volatile and non-volatile flavour mixtures, 179

Cluster

A semi-empirical concept for the calculation of electron-impact ionization cross-sections of neutral and ionized fullerenes, 1
Low energy (0–15 eV) electron stimulated reactions in single 1,2-C₂F₄Cl₂ molecules and clusters, 193

Calculations of partial electron-impact cross sections for the multiple ionization of fullerenes using a semi-empirical method, 253

The relationship between covariance and anti-covariance mapping, 355

A semi-empirical method for the calculation of cross sections for the electron-impact ionization of negatively charged fullerenes, 703

Cluster ions

Atmospheric pressure chemical ionization mass spectrometry for the detection of tropospheric trace gases: the influence of clustering on sensitivity and precision, 771

Coffee aroma

Analysing the headspace of coffee by proton-transfer-reaction mass-spectrometry, 115

Coffee brew

Analysing the headspace of coffee by proton-transfer-reaction mass-spectrometry, 115

Collision

Stark mixing in Rydberg atoms by ultralow energy collisions with ions, 473

Bond-forming reactivity between CF₃²⁺ and H₂/D₂, 547

Column liquid chromatography

Analysis of isolectins on non-porous particles and monolithic polystyrene-divinylbenzene based stationary phases and electrospray ionization mass spectrometry, 519

Combined ion mass and energy analyzer

Interpretation of ion distribution functions measured by a combined energy and mass analyzer, 679

Combustion chamber

Combustion and carbonisation exhaust utilisation in electric discharge and its relation to prebiotic chemistry, 613

Coronene

The gas-phase chemistry of iron cations coordinated to benzene and the extended aromatic coronene, 411

Coulomb explosion

The relationship between covariance and anti-covariance mapping, 355

Covariance mapping

The relationship between covariance and anti-covariance mapping, 355

Cross section calculations

Calculated absolute cross section for the electron-impact ionisation of simple molecular ions, 639

Cross-section

Effect of temperature on dissociative electron attachment to CCl₂F₂, 217

Production of Cl[−] via dissociative electron attachment to Cl₂, 661

Cyanogenesis

Negative-ion CIMS: analysis of volatile leaf wound compounds including HCN, 427

Dication

Bond-forming reactivity between CF₃²⁺ and H₂/D₂, 547

Diffusion coefficient

Membrane introduction proton-transfer reaction mass spectrometry, 763

Dissociative electron attachment

Temperature dependencies in dissociative electron attachment to CCl₄, CCl₂F₂, CHCl₃ and CHBr₃, 9

DM

Calculation of electron impact ionization cross sections of DNA using the Deutsch–Märk and Binary–Encounter–Bethe formalisms, 599

DMSO

Ab initio study of the interaction of dimethylsulfoxide with the ions Li⁺ and I[−], 263

DMSO–I[−] complex

Ab initio study of the interaction of dimethylsulfoxide with the ions Li⁺ and I[−], 263

DMSO–Li⁺ complex

Ab initio study of the interaction of dimethylsulfoxide with the ions Li⁺ and I[−], 263

DNA

Calculation of electron impact ionization cross sections of DNA using the Deutsch–Märk and Binary–Encounter–Bethe formalisms, 599

DNA damage

Modeling of ultrasoft X-ray induced DNA damage using structured higher order DNA targets, 579

Drift tube pressure

Proton transfer reaction mass spectrometry at high drift tube pressure, 507

Dusty plasma

Plasma–powder interaction: trends in applications and diagnostics, 313

Electron

A three-step model applied to free electron attachment to C₆₀, Buckminsterfullerene, 447

Electron attachment

Low energy (0–15 eV) electron stimulated reactions in single 1,2-C₂F₄Cl₂ molecules and clusters, 193

Effect of temperature on dissociative electron attachment to CCl₂F₂, 217

Production of Cl[−] via dissociative electron attachment to Cl₂, 661

Electron attachment cross section

The ion extraction efficiency in a crossed beams experiment using a trochoidal electron monochromator, 271

Electron energy loss

VUV and low energy electron impact study of electronic state spectroscopy of CF₃I, 647

Electron impact

A semi-empirical concept for the calculation of electron-impact ionization cross-sections of neutral and ionized fullerenes, 1

- Calculations of partial electron-impact cross sections for the multiple ionization of fullerenes using a semi-empirical method, 253
- Calculation of electron impact ionization cross sections of DNA using the Deutsch–Märk and Binary–Encounter–Bethe formalisms, 599
- A semi-empirical method for the calculation of cross sections for the electron-impact ionization of negatively charged fullerenes, 703
- Electron monochromator**
- The ion extraction efficiency in a crossed beams experiment using a trochoidal electron monochromator, 271
- Electron scattering**
- Low-energy electron collisions in nitrogen oxides: a comparative study, 205
- Electron transfer**
- Reactions between CH_4^+ and $\text{C}_2\text{H}_5\text{OH}$, 81
- State selectivity in collisional electron-transfer processes involving the NO molecule, 169
- Bond-forming reactivity between CF_3^{2+} and H_2/D_2 , 547
- Electronic and infrared spectra**
- Electronic and infrared absorption spectra of NCCN^+ , 107
- Electron-impact ionisation**
- Calculated absolute cross section for the electron-impact ionisation of simple molecular ions, 639
- Electron–molecule interactions**
- Temperature dependencies in dissociative electron attachment to CCl_4 , CCl_2F_2 , CHCl_3 and CHBr_3 , 9
- Electrospray ionization (ESI) mass spectrometry**
- Analysis of isolectins on non-porous particles and monolithic polystyrene-divinylbenzene based stationary phases and electrospray ionization mass spectrometry, 519
- Endohedral**
- Mass spectrometric study of $\text{K}^+ + \text{C}_{60}$ collisions, 695
- Energy transfer**
- Dynamics of hyperthermal energy ion–surface collisions: dissociative and non-dissociative scattering of ethanol cations from a self-assembled monolayer surface of fluorinated alkyl thiol on Au (1 1), 783
- ESI**
- An electrospray ionization—flow tube study of H/D exchange in protonated serine, 491
- Ethanol ions**
- Dynamics of hyperthermal energy ion–surface collisions: dissociative and non-dissociative scattering of ethanol cations from a self-assembled monolayer surface of fluorinated alkyl thiol on Au (1 1), 783
- Ethylene**
- A photoionization mass spectrometric study of acetylene and ethylene in the VUV spectral region, 67
- Excimers**
- Neon excimer emission from pulsed high-pressure microhollow cathode discharge plasmas, 37
- Excitation**
- The influence of electron impact ionisations on low frequency instabilities in a magnetised plasma, 141
- Exhaust cleaning**
- Combustion and carbonisation exhaust utilisation in electric discharge and its relation to prebiotic chemistry, 613
- Femtosecond laser**
- The relationship between covariance and anti-covariance mapping, 355
- Fertiliser**
- Combustion and carbonisation exhaust utilisation in electric discharge and its relation to prebiotic chemistry, 613
- Flow tube**
- An electrospray ionization—flow tube study of H/D exchange in protonated serine, 491
- Fluoranthene**
- Experimental evaluation of the recombination rate of cations formed from fluoranthene, 237
- Fragmentation**
- Analysing the headspace of coffee by proton-transfer-reaction mass-spectrometry, 115
- Freon**
- Effect of temperature on dissociative electron attachment to CCl_2F_2 , 217
- FT-MS**
- Radiative lifetime of vibrationally excited N_2H^+ and N_2D^+ molecular ions, 669
- Fullerenes**
- A semi-empirical concept for the calculation of electron-impact ionization cross-sections of neutral and ionized fullerenes, 1
- Calculations of partial electron-impact cross sections for the multiple ionization of fullerenes using a semi-empirical method, 253
- A semi-empirical method for the calculation of cross sections for the electron-impact ionization of negatively charged fullerenes, 703
- Gas discharge**
- Combustion and carbonisation exhaust utilisation in electric discharge and its relation to prebiotic chemistry, 613
- Gas sampling probe**
- Limitations in the time resolution of quadrupole mass spectrometry using a flushed extraction probe, 301
- Gas-phase enantioselectivity**
- Gas-phase complexes: noncovalent interactions and stereospecificity, 159
- GC–FID**
- Evaluation of three gas chromatography and two direct mass spectrometry techniques for aroma analysis of dried red bell peppers, 55
- Measurement of monoterpenes and related compounds by proton transfer reaction-mass spectrometry (PTR-MS), 561
- GC–MS**
- Evaluation of three gas chromatography and two direct mass spectrometry techniques for aroma analysis of dried red bell peppers, 55
- GC–O**
- Evaluation of three gas chromatography and two direct mass spectrometry techniques for aroma analysis of dried red bell peppers, 55
- Graphite**
- Edge plasma-relevant ion–surface collision processes, 21
- H/D exchange**
- An electrospray ionization—flow tube study of H/D exchange in protonated serine, 491

- Halogenated hydrocarbon
Reactions of H_3O^+ with a number of bromine containing fully and partially halogenated hydrocarbons, 627
- Headspace
Analysing the headspace of coffee by proton-transfer-reaction mass-spectrometry, 115
- Headspace analysis
Membrane introduction proton-transfer reaction mass spectrometry, 763
- Headspace of meat
Detection of the spoiling of meat using PTR-MS, 229
- Heavy radionuclides
Accelerator mass spectrometry of heavy long-lived radionuclides, 713
- High temperature flowing afterglow
A reexamination of the temperature dependence of the reaction of N^+ with O_2 , 397
- High-pressure plasmas
Neon excimer emission from pulsed high-pressure microhollow cathode discharge plasmas, 37
- HLC
Dynamic measurements of partition coefficients using proton-transfer-reaction mass spectrometry (PTR-MS), 383
- Hollow cathode discharges
Neon excimer emission from pulsed high-pressure microhollow cathode discharge plasmas, 37
- Humidity interference
Atmospheric pressure chemical ionization mass spectrometry for the detection of tropospheric trace gases: the influence of clustering on sensitivity and precision, 771
- Hydroxide anion
Negative-ion CIMS: analysis of volatile leaf wound compounds including HCN, 427
- Inelastic collisions
Dynamics of hyperthermal energy ion-surface collisions: dissociative and non-dissociative scattering of ethanol cations from a self-assembled monolayer surface of fluorinated alkyl thiol on Au (1 1 1), 783
- Insertion threshold
Mass spectrometric study of $\text{K}^+ + \text{C}_{60}$ collisions, 695
- Ion distribution function
Interpretation of ion distribution functions measured by a combined energy and mass analyzer, 679
- Ion extraction efficiency
The ion extraction efficiency in a crossed beams experiment using a trochoidal electron monochromator, 271
- Ion trajectory simulations
Ion optics evaluation of the plasma ion mass spectrometer (PIMS) designed for the JET tokamak, 45
- Ion vibrational relaxation
Vibrational quenching of $\text{NO}^+(\nu)$ ions by Ar collisions, 757
- Ionisation
The influence of electron impact ionisations on low frequency instabilities in a magnetised plasma, 141
- Ionization cross sections
A semi-empirical concept for the calculation of electron-impact ionization cross-sections of neutral and ionized fullerenes, 1
Calculations of partial electron-impact cross sections for the multiple ionization of fullerenes using a semi-empirical method, 253
Calculation of electron impact ionization cross sections of DNA using the Deutsch-Märk and Binary-Encounter-Bethe formalisms, 599
A semi-empirical method for the calculation of cross sections for the electron-impact ionization of negatively charged fullerenes, 703
- Ion-molecule reaction
A selected ion flow tube investigation of the positive ion chemistry of a number of bromine containing fully and partially halogenated hydrocarbons, 91
Selected ion flow tube study of NH_4^+ association and of product switching reactions with a series of organic molecules, 459
The reaction of SiH^+ and SH^+ with small molecules, 539
- Ions
Experimental evaluation of the recombination rate of cations formed from fluoranthene, 237
- Ion-surface collisions
Dynamics of hyperthermal energy ion-surface collisions: dissociative and non-dissociative scattering of ethanol cations from a self-assembled monolayer surface of fluorinated alkyl thiol on Au (1 1 1), 783
- Iron cation
The gas-phase chemistry of iron cations coordinated to benzene and the extended aromatic coronene, 411
- Isoforms
Analysis of isolectins on non-porous particles and monolithic polystyrene-divinylbenzene based stationary phases and electrospray ionization mass spectrometry, 519
- Isomerization
Surface collisions of the acetonitrile molecular ion: evidence for isomerization of $\text{CD}_3\text{CN}^{*+}$ to the ketenimine cation $\text{CD}_2=\text{C}=\text{ND}^{*+}$, 279
- Isotope effect
Bond-forming reactivity between CF_3^{2+} and H_2/D_2 , 547
- Lectins
Analysis of isolectins on non-porous particles and monolithic polystyrene-divinylbenzene based stationary phases and electrospray ionization mass spectrometry, 519
- Ligation
The gas-phase chemistry of iron cations coordinated to benzene and the extended aromatic coronene, 411
- Low-pressure plasma
Plasma-powder interaction: trends in applications and diagnostics, 313
- Mass spectrometry
Gas-phase complexes: noncovalent interactions and stereospecificity, 159
State selectivity in collisional electron-transfer processes involving the NO molecule, 169
Low energy (0–15 eV) electron stimulated reactions in single 1,2- $\text{C}_2\text{F}_4\text{Cl}_2$ molecules and clusters, 193

- Limitations in the time resolution of quadrupole mass spectrometry using a flushed extraction probe, 301
- Meat storage**
Detection of the spoiling of meat using PTR-MS, 229
- Membrane**
Membrane introduction proton-transfer reaction mass spectrometry, 763
- Metal atoms**
Reactions of trapped ions with metal atoms: O_2^+ + Ni and NiN_2^+ + Ni, 291
- Metal clusters**
Gas-phase complexes: noncovalent interactions and stereospecificity, 159
- Metallofullerene**
Mass spectrometric study of K^+ + C_{60} collisions, 695
- Metastable atoms**
The charge-excitation exchange process: $He^+(^2S) + Ar^*(^3P) \rightarrow He^*(^3^1S) + Ar^+(^2P)$, 327
- Molecular ion structures**
Selected ion flow tube study of NH_4^+ association and of product switching reactions with a series of organic molecules, 459
- Molecular ions**
Calculated absolute cross section for the electron-impact ionisation of simple molecular ions, 639
- Monitor ion technique**
Radiative lifetime of vibrationally excited N_2H^+ and N_2D^+ molecular ions, 669
- Monoterpene**
Measurement of monoterpene and related compounds by proton transfer reaction-mass spectrometry (PTR-MS), 561
- Monte Carlo simulation**
Modeling of ultrasoft X-ray induced DNA damage using structured higher order DNA targets, 579
- Multiply charged ion**
Edge plasma-relevant ion-surface collision processes, 21
- NCCN⁺**
Electronic and infrared absorption spectra of NCCN⁺, 107
- N₂D⁺**
Radiative lifetime of vibrationally excited N_2H^+ and N_2D^+ molecular ions, 669
- Negative ions**
Low energy (0–15 eV) electron stimulated reactions in single 1,2-C₂F₄Cl₂ molecules and clusters, 193
- Negative-ion chemical-ionization**
Negative-ion CIMS: analysis of volatile leaf wound compounds including HCN, 427
- Neutralization–reionization**
State selectivity in collisional electron-transfer processes involving the NO molecule, 169
- N₂H⁺**
Radiative lifetime of vibrationally excited N_2H^+ and N_2D^+ molecular ions, 669
- Nitrogen monoxide**
State selectivity in collisional electron-transfer processes involving the NO molecule, 169
- Nitrogen oxide**
Low-energy electron collisions in nitrogen oxides: a comparative study, 205
- NO^{+(v)}**
Vibrational quenching of NO^{+(v)} ions by Ar collisions, 757
- Non-elastic scattering**
Vibrational relaxation in $H_2 + H_2$: full-dimensional quantum dynamical study, 335
- Non-linear interaction**
The influence of electron impact ionisations on low frequency instabilities in a magnetised plasma, 141
- Non-porous and monolithic polystyrene-divinylbenzene**
Analysis of isolectins on non-porous particles and monolithic polystyrene-divinylbenzene based stationary phases and electrospray ionization mass spectrometry, 519
- Non-volatile mixture**
Direct mass spectrometry of complex volatile and non-volatile flavour mixtures, 179
- On-line analysis**
Analysing the headspace of coffee by proton-transfer-reaction mass-spectrometry, 115
- Oxygenated hydrocarbons**
Detection of gaseous oxygenated hydrocarbons in upper tropospheric and lower stratospheric aircraft borne experiments, 733
- Ozone**
The ion extraction efficiency in a crossed beams experiment using a trochoidal electron monochromator, 271
- Partition coefficients**
Analysing the headspace of coffee by proton-transfer-reaction mass-spectrometry, 115
- Pasteurisation**
Fingerprinting mass spectrometry by PTR-MS: heat treatment vs. pressure treatment of red orange juice—a case study, 343
- PEPICO**
Reactions between CH_4^+ and C_2H_5OH , 81
- Perfluorocarbons**
Reactions of H_3O^+ with a number of bromine containing fully and partially halogenated hydrocarbons, 627
- Photoionization**
A photoionization mass spectrometric study of acetylene and ethylene in the VUV spectral region, 67
- Plasma instabilities**
The influence of electron impact ionisations on low frequency instabilities in a magnetised plasma, 141
- Plasma mass spectrometry**
Ion optics evaluation of the plasma ion mass spectrometer (PIMS) designed for the JET tokamak, 45
- Plasma–particle interaction**
Plasma–powder interaction: trends in applications and diagnostics, 313
- Plasma–surface interaction**
Edge plasma-relevant ion-surface collision processes, 21
- Positive ion chemistry**
A selected ion flow tube investigation of the positive ion chemistry of a number of bromine containing fully and partially halogenated hydrocarbons, 91

- Potential energy surface
 Electronic and infrared absorption spectra of NCCN^+ , 107
 Vibrational relaxation in $\text{H}_2 + \text{H}_2$: full-dimensional quantum dynamical study, 335
- Proton transfer
 Reactions between CH_4^+ and $\text{C}_2\text{H}_5\text{OH}$, 81
- Proton transfer reaction-mass spectrometry, PTR-MS
 Analysing the headspace of coffee by proton-transfer-reaction mass-spectrometry, 115
- Fingerprinting mass spectrometry by PTR-MS: heat treatment vs. pressure treatment of red orange juice—a case study, 343
 Sensitivity and specificity of atmospheric trace gas detection by proton-transfer-reaction mass spectrometry, 365
 Dynamic measurements of partition coefficients using proton-transfer-reaction mass spectrometry (PTR-MS), 383
 Proton transfer reaction mass spectrometry at high drift tube pressure, 507
 Trace gas monitoring at the Mauna Loa Baseline Observatory using Proton-Transfer Reaction Mass Spectrometry, 527
 Measurement of monoterpenes and related compounds by proton transfer reaction-mass spectrometry (PTR-MS), 561
 Membrane introduction proton-transfer reaction mass spectrometry, 763
- PTR-MS
 Evaluation of three gas chromatography and two direct mass spectrometry techniques for aroma analysis of dried red bell peppers, 55
 Breath-by-breath analysis of banana aroma by proton transfer reaction mass spectrometry, 743
- PTR-MS mass spectrometry
 Detection of the spoiling of meat using PTR-MS, 229
- Pyridine clusters
 The relationship between covariance and anti-covariance mapping, 355
- Pyrolysis
 Combustion and carbonisation exhaust utilisation in electric discharge and its relation to prebiotic chemistry, 613
- Radiative lifetimes
 Radiative lifetime of vibrationally excited N_2H^+ and N_2D^+ molecular ions, 669
- Rate coefficients
 Selected ion flow tube study of NH_4^+ association and of product switching reactions with a series of organic molecules, 459
- Rate constant
 A reexamination of the temperature dependence of the reaction of N^+ with O_2 , 397
- Reaction rate coefficient
 The reaction of SiH^+ and SH^+ with small molecules, 539
- Recombination
 Experimental evaluation of the recombination rate of cations formed from fluoranthene, 237
- Red orange juice
 Fingerprinting mass spectrometry by PTR-MS: heat treatment vs. pressure treatment of red orange juice—a case study, 343
- Resonances
 Low energy (0–15 eV) electron stimulated reactions in single 1,2- $\text{C}_2\text{F}_4\text{Cl}_2$ molecules and clusters, 193
- Ring electrode trap
 Reactions of trapped ions with metal atoms: $\text{O}_2^+ + \text{Ni}$ and $\text{NiN}_2^+ + \text{Ni}$, 291
- Rydberg atoms
 Stark mixing in Rydberg atoms by ultralow energy collisions with ions, 473
- Scattering
 Dynamics of hyperthermal energy ion–surface collisions: dissociative and non-dissociative scattering of ethanol cations from a self-assembled monolayer surface of fluorinated alkyl thiol on $\text{Au} (1\ 1\ 1)$, 783
- Selected ion flow drift tube
 Vibrational quenching of $\text{NO}^+(v)$ ions by Ar collisions, 757
- Selected ion flow tube
 A reexamination of the temperature dependence of the reaction of N^+ with O_2 , 397
 Negative-ion CIMS: analysis of volatile leaf wound compounds including HCN , 427
- Self-assembled monolayer surface
 Dynamics of hyperthermal energy ion–surface collisions: dissociative and non-dissociative scattering of ethanol cations from a self-assembled monolayer surface of fluorinated alkyl thiol on $\text{Au} (1\ 1\ 1)$, 783
- SH^+
 The reaction of SiH^+ and SH^+ with small molecules, 539
- Sidebands
 The influence of electron impact ionisations on low frequency instabilities in a magnetised plasma, 141
- SIFT
 A selected ion flow tube investigation of the positive ion chemistry of a number of bromine containing fully and partially halogenated hydrocarbons, 91
 A temperature-dependent selected ion flow tube study of anions reacting with SF_5CF_3 , 403
 Selected ion flow tube study of NH_4^+ association and of product switching reactions with a series of organic molecules, 459
- SiH^+
 The reaction of SiH^+ and SH^+ with small molecules, 539
- Site-specific rate constants
 An electrospray ionization—flow tube study of H/D exchange in protonated serine, 491
- Solvation effects
 Low energy (0–15 eV) electron stimulated reactions in single 1,2- $\text{C}_2\text{F}_4\text{Cl}_2$ molecules and clusters, 193
- Spectroscopy
 VUV and low energy electron impact study of electronic state spectroscopy of CF_3I , 647
- Stark mixing
 Stark mixing in Rydberg atoms by ultralow energy collisions with ions, 473
- Structured target
 Modeling of ultrasoft X-ray induced DNA damage using structured higher order DNA targets, 579

Surface reactions

Surface collisions of the acetonitrile molecular ion: evidence for isomerization of CD_3CN^+ to the ketenimine cation $\text{CD}_2=\text{C}=\text{ND}^+$, 279

Surface-induced dissociation

Dynamics of hyperthermal energy ion–surface collisions: dissociative and non-dissociative scattering of ethanol cations from a self-assembled monolayer surface of fluorinated alkyl thiol on Au (1 1 1), 783

Switching reactions

Selected ion flow tube study of NH_4^+ association and of product switching reactions with a series of organic molecules, 459

Synchrotron radiation

UV and low energy electron impact study of electronic state spectroscopy of CF_3I , 647

Tandem mass spectrometry

Surface collisions of the acetonitrile molecular ion: evidence for isomerization of CD_3CN^+ to the ketenimine cation $\text{CD}_2=\text{C}=\text{ND}^+$, 279

Temperature dependence

Effect of temperature on dissociative electron attachment to CCl_2F_2 , 217

Temperature dependencies

Temperature dependencies in dissociative electron attachment to CCl_4 , CCl_2F_2 , CHCl_3 and CHBr_3 , 9

Time resolution

Limitations in the time resolution of quadrupole mass spectrometry using a flushed extraction probe, 301

Time-of-flight mass spectrometer

The relationship between covariance and anti-covariance mapping, 355

Tokamak plasma

Ion optics evaluation of the plasma ion mass spectrometer (PIMS) designed for the JET tokamak, 45

Total ion current

Interpretation of ion distribution functions measured by a combined energy and mass analyzer, 679

Trace gas monitoring

Trace gas monitoring at the Mauna Loa Baseline Observatory using Proton-Transfer Reaction Mass Spectrometry, 527

Trapped ions

Reactions of trapped ions with metal atoms: $\text{O}_2^+ + \text{Ni}$ and $\text{NiN}_2^+ + \text{Ni}$, 291

Trifluoromethyl sulfurpentafluoride

A temperature-dependent selected ion flow tube study of anions reacting with SF_3CF_3 , 403

Trochoidal mass spectrometer

Ion optics evaluation of the plasma ion mass spectrometer (PIMS) designed for the JET tokamak, 45

Tropospheric chemistry

Atmospheric pressure chemical ionization mass spectrometry for the detection of tropospheric trace gases: the influence of clustering on sensitivity and precision, 771

UT

Detection of gaseous oxygenated hydrocarbons in upper tropospheric and lower stratospheric aircraft borne experiments, 733

UVX irradiation

Modeling of ultrasoft X-ray induced DNA damage using structured higher order DNA targets, 579

VERA

Accelerator mass spectrometry of heavy long-lived radionuclides, 713

Vibrational relaxation

Vibrational relaxation in $\text{H}_2 + \text{H}_2$: full-dimensional quantum dynamical study, 335

Volatile mixture

Direct mass spectrometry of complex volatile and non-volatile flavour mixtures, 179

Volatile organic compounds

Detection of the spoiling of meat using PTR-MS, 229

Fingerprinting mass spectrometry by PTR-MS: heat treatment vs. pressure treatment of red orange juice—a case study, 343

Sensitivity and specificity of atmospheric trace gas detection by proton-transfer-reaction mass spectrometry, 365

Dynamic measurements of partition coefficients using proton-transfer-reaction mass spectrometry (PTR-MS), 383

Negative-ion CIMS: analysis of volatile leaf wound compounds including HCN, 427

Trace gas monitoring at the Mauna Loa Baseline Observatory using Proton-Transfer Reaction Mass Spectrometry, 527

VUV absorption

UV and low energy electron impact study of electronic state spectroscopy of CF_3I , 647